



# Development of epoxy resin-based microfluidic devices using CO<sub>2</sub> laser ablation for DNA amplification point-of-care (POC) applications

Heba Mansour<sup>1,2</sup> · Emad A. Soliman<sup>2</sup> · Ahmed M. Fath El-Bab<sup>3</sup> · Ahmed L. Abdel-Mawgood<sup>1</sup>

Received: 19 November 2021 / Accepted: 26 February 2022 / Published online: 15 March 2022  
© The Author(s) 2022

## Abstract

Microfluidic devices are a rising technology to automatize chemical and biological operations. In this context, laser ablation has significant potential for polymer-based microfluidic platforms' fast and economical manufacturing. Nevertheless, the manufacturing of epoxy-based microfluidic chips is considered highly cost full due to the demand for cleanroom facilities that utilize expensive equipment and lengthy processes. Therefore, this study targeted investigating the feasibility of epoxy resins to be fabricated as a lab-on-chip using carbon dioxide laser ablation. The chemical structural properties and thermal stability of the plain epoxy resins were characterized by Fourier transform infrared spectral analysis (FT-IR) and thermogravimetric analysis (TGA). Moreover, a specific migration test was performed to quantify potential migrants by gas chromatography coupled to mass spectrometry (GC-MS) to prove that the cured epoxy resin would not release unreacted monomers to the biological solution test, which caused inhibition of the sensitive biological reactions. By investigating the impact of this process on microchannels' dimensions and quality, a laser technique using CO<sub>2</sub> laser was used in vector mode to engrave into a transparent epoxy resin chip. The resulting microchannels were characterized using 3D laser microscopy. The outcomes of this study showed considerable potential for laser ablation in machining the epoxy-based chips, whereas the microchannels machined by laser processing at an input power of 1.8 W and scanning speed of 5 mm/s have an aspect ratio of about 1.19 and a reasonable surface roughness (Ra) of ~ 15 μm. Meanwhile, the bulge height was 0.027 μm with no clogging, and HAZ was ~ 18 μm. This study validated the feasibility of quick and cost-effective CO<sub>2</sub> laser microfabrication to develop epoxy resin-based microfluidic chips without the need for cleanroom facilities that require expensive equipment and lengthy process.

**Keywords** Epoxy-based chips · CO<sub>2</sub> laser ablation · Microchannel dimensions · Microchannel quality · Microfluidics · Micromachining

## 1 Introduction

During the past few decades, advances in microfabrication and nanotechnologies enabled the development of analytical devices characterized by new capabilities and small sizes practical for diagnostic, pharmaceutical, analytical, and medical industries. Miniaturization of analytical devices has reduced sample and reagents consumption, in addition to new functionality; enhanced the sensitivity; and reduced the time and cost than that of conventional analytical techniques [1]. Microfluidic chips are one of these miniaturized devices that have emerged as a promising technology recently in

the last two decades. It has proved its competence astonishingly. Therefore, it experienced exponential developmental growth and became a prevailing tool with vast potential [2]. Microfluidic devices can be broadly defined pertaining to systems that manipulate or process small quantities of fluids (10<sup>-9</sup> to 10<sup>-18</sup> L), using microchannels of tens to hundreds of micrometres in dimensions [3, 4]. More comprehensively, microfluidic devices are usually made up of miniaturized manipulation flow and fluid components, for instance, microchannels, micropumps, micromixers, and microvalves [5]. These miniaturized components forming the microfluidic chips are implemented and integrated with analytical and detection approaches such as chromatography, electrophoresis, fluorescence, and electrochemical detection) on microfabricated platforms to achieve the desired features such as on-chip reaction (microreactor), cell culture

✉ Heba Mansour  
heba.mansour@ejust.edu.eg

Extended author information available on the last page of the article

(organ-on-a-chip), or on-chip analysis, i.e. separation and detection of various compounds or pathogens (lab-on-a-chip) [6].

It is worth mentioning that the microchannel particularities are greatly affected by the material type and microfabrication techniques. Therefore, choosing the optimum material for the device fabrication process is one of the fundamental steps in microfluidic technology [2, 7]. Specific essential properties must be considered when selecting the material, such as durability, biocompatibility, transparency, chemical compatibility with the implied reagents, ease of fabrication, withstanding the pressure and temperature conditions required for the reaction, and the feasibility of surface functionalization [7].

Numerous classes of materials were developed to match such properties and can be used to manufacture microfluidic devices. Typical substrates include glass, silicon, metals, polymers, and ceramics. However, each material has advantages and disadvantages, depending on its destination application. Polymers are broadly used in manufacturing microfluidic devices because of the diversity of the materials and the ability of chemical modification, providing a wide range of surface/material properties. There are various methods available for device fabrication, including casting, hot embossing, injection molding, soft lithography, micromachining, etching, and laser ablation, in addition to lower cost with strong bio-chemical performances [2]. So far, polydimethylsiloxane (PDMS), polymethylmethacrylate (PMMA), fluoropolymers, cyclo-olefin polymers, copolymers (COPs/COCs), and thiolene polymers (TEs) are the most commonly used polymers for microfluidic device manufacturing [8].

Epoxy resin is an oligomer with a three-dimensional crosslinked network solidified by hardeners to form thermosetting plastics [9]. Owing to the superior characteristics of epoxy resins, they are considered significant engineering materials and are widely utilized in structural applications and protecting coatings [2]. Epoxy resins are among the most important thermosetting polymers that have attracted considerable attention in microfluidic technology because of their exceptional biocompatibility, good mechanical, chemical resistance, thermal stability, and toughness [9].

Remarkably, indirect fabrication techniques like photolithographic techniques require the generation of masks and transforming strategies that need the fabrication of master molds. These techniques have lower flexibility and add a step to the microfluidic chips fabrication process, requiring access to clean-room facilities [10].

Microfluidic device creation using lasers has become a robust technology. CO<sub>2</sub> laser ablation provides several advantages, including low cost, quick prototyping time, and no requirement for chemicals or cleanroom facilities. Laser engraving has much potential for making polymeric microfluidic devices quickly and cheaply [11]. Glass, quartz,

PDMS, polytetrafluoroethylene (PTFE), polycarbonate (PC), polystyrene (PS), cyclic olefin copolymer (COC), laminates, and paper have all been used in CO<sub>2</sub> laser patterning [12]. There is no study in the literature that we are aware of that uses applying CO<sub>2</sub> laser ablation to epoxy resin. This process can produce epoxy resin-based microfluidic chips without needing cleanroom facilities requiring expensive equipment and lengthy procedures.

As a result, researchers are still seeking novel materials and inventing new fabrication processes to suit the criteria of high flexibility, quick turn-around, and low cost in producing microfluidic devices. Such requirements are considered a stepping stone along the pathway towards commercialization. Therefore, in this study, the casting method and CO<sub>2</sub> laser micromachining were used to develop cured epoxy resin-based microfluidic devices that could be rapidly prototyped for molecular diagnosis (DNA amplification point-of-care (POC)) applications. Moreover, the impact of laser micromachining parameters, including laser power (P) and scanning speed (U) on the microchannel dimensions and roughness and heat defects, was investigated.

## 2 Microfabrication

The most mature shaping and microfabrication technologies of thermoplastic polymers differ significantly from those for thermoset polymers. Whereas thermoplastic polymers already have a high molecular weight, thermoset polymers are crosslinked networks formed from low molecular weight components. For prototyping and low-volume device fabrication, thin thermoset epoxy resin chips are formed using casting technique, followed by direct patterning onto a thermosetting substrate using laser ablation without generating an expensive molding master and undertaking the time-consuming process.

### 2.1 Casting technique

For this experiment, epoxy resin (diglycidyl ether of bisphenol-A (DGEBA) (epoxide equivalent mass of the resin (185–190)) and curing agent (modified cyclo-aliphatic polyamine) were purchased from Green Build Chemical Company (Egypt). Conventionally, the epoxy elastomer could be obtained by modulating the cured three-dimensional networks' crosslinking density via adjusting the curing agents' proportion and the condition of the curing process. Therefore, epoxy resin and curing agent (hardener) were mixed at a ratio of 2:1.25 that was selected based on our preliminary work. The mixture was mechanically stirred for 20 min followed by degassing in a vacuum oven at 25 °C for 20 min to remove the bubbles before their casting into Si moulds. The cast resin was left at room temperature overnight to accomplish the curing process. The

cured epoxy resin-based chips were optically transparent with a tensile modulus of 30.38 MPa. Their surfaces were characterized with a hydrophobic nature with a contact angle of 107°.

## 2.2 Laser micromachining setup

The CO<sub>2</sub> laser ablation is a physical process in which the infrared radiation emitted by the focused CO<sub>2</sub> laser beam continuously ablates the materials. This process has been recently used to fabricate various polymer microsystems such as microfluidic channels and microlenses. Therefore, CO<sub>2</sub> laser ablation was utilized in this study to fabricate an epoxy resin-based microfluidic device. This was conducted by drawing the desired microchannel pattern on the pre-cast transparent cured epoxy resin-based chip (thickness = 3 mm) using a commercial benchtop CO<sub>2</sub> laser system (Universal Laser System, VLS 3.5, USA) demonstrated schematically in Fig. 1. The radio-frequency excited CO<sub>2</sub> laser has a wavelength of 10.6 μm with a maximum power of 30 W. The desired pattern was designed and imported to the laser system using CorelDrawX5 2010 and laser system programmes associated with computer-aided design (CAD) plotter, which offers the function to set the processing parameters, including laser power and the scanning speed. The CO<sub>2</sub> laser system programme has two modes that can be used depending on the width of the lines in the layout. The first is vector engraving for line widths less than 200 μm, and the second is raster engraving greater than 200 μm. The laser source follows a two-dimensional path based on the established CAD pattern in a vector engraving manner, whereas, in raster engraving mode, the designed pattern image is divided into an array of dots (with a resolution of up to 1000 dpi) for engraving in raster engraving mode [13]. This CAD plotter can accommodate eight different laser settings in one pass; the design was plotted on eight lines at a time. The laser micromachining was accomplished with a 50-mm (2

in.) lens for focusing the laser beam at a focal distance of 5062.5 mm at laser power was varied from 1.8 to 5.4 W at a scanning speed ranging from 5 to 40 mm/s. The pulse rate was set at 1000 PPI, as listed in Table 1. To optimize these process parameters, the peculiarities of the microchannel of the resulting epoxy resin microfluidic chips, including width and depth of the microchannel, surface roughness (Ra), and bulge heights, were characterized using a 3D laser microscope (KEYENCE VK-×100). Photographs of the fabricated epoxy resin-based microfluidic chips with the proposed pattern composed of the most commonly used microchannel shapes are shown in Fig. 2.

## 3 Characterization of epoxy resin and its based chips

To assure the potential feasibility of the thermosetting epoxy resin substrate for microfluidic application, the structural and thermal properties of epoxy resin, as well as overall and specific migration and autoclaving endurance, were assessed as shown in the following methods.

### 3.1 Fourier transform infrared (FT-IR) spectral analysis

The chemical structure of epoxy resin and cured epoxy resin was studied by Fourier transform infrared (FT-IR) spectral analysis. FTIR spectra were registered on a Shimadzu FTIR-8400S spectrometer in a range of 400–4000 cm<sup>-1</sup> at a resolution of 4 cm<sup>-1</sup> and 32 scans. The samples were analysed in KBr pellets.

### 3.2 Thermogravimetric analysis (TGA)

The thermal stability of cured epoxy resin was assessed using Shimadzu TGA-50 thermogravimetric analyser via heating the specimen from ambient temperature to 600 °C at a rate of 10 °C/min under nitrogen atmosphere.

### 3.3 Overall and specific migration determination

To explore that the cured epoxy resin would not release any migrants that can cause inhibition of the sensitive biological samples and subsequently loss of the test accuracy and microfluidic chips efficiency. Overall and specific migration was determined according to the method of Cardama and others [15]. Briefly, to extract the migrants, a known surface of the epoxy resin specimen was put in contact with a definite volume of the distilled water for 2 h on a magnetic stirrer at 100 °C, then an aliquot of the extracts (2 mL) was evaporated. The remaining were weighted in a sensitive balance then dispersed in 2 mL methanol. Finally, the resultant solution was analysed to identify potential migrants by gas

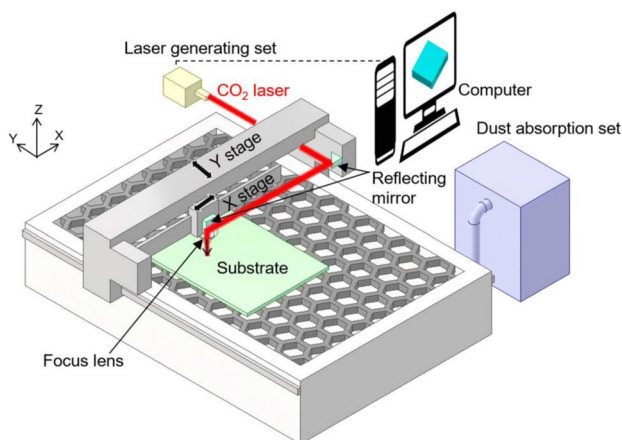


Fig. 1 Schematic illustration of CO<sub>2</sub> laser ablation process [14]

**Table 1** Applied CO<sub>2</sub> laser ablation process parameters

Process parameter	Values								
Laser power (W)	1.8	2.4	3	3.6	4.2	4.8	5.4		
Laser speed (mm/s)	5	7.5	10	12.5	15	17.5	20	30	40

chromatography coupled with mass spectrometer GC–MS (Shimadzu GC–MS-QP2010). Moreover, the procedures have been conducted by using another simulant with lower polarity, dichloromethane, to investigate its potency for releasing the migratable substances from epoxy resin.

### 3.3.1 Autoclaving endurance

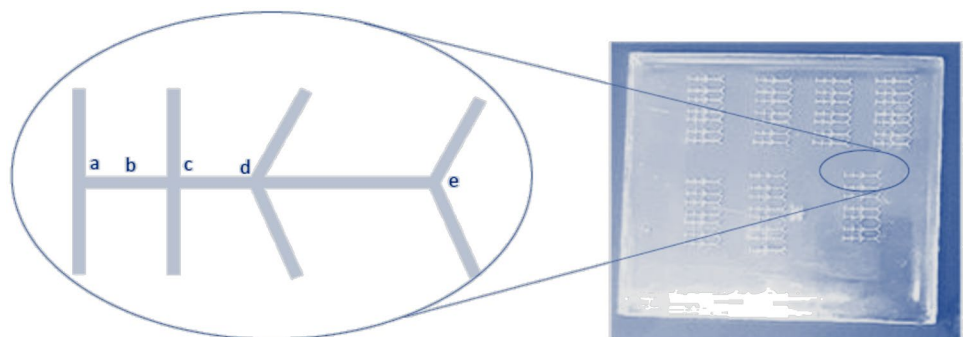
Sterilization is a vital process for all materials or devices used in analytical and biomedical applications, particularly those which deal with biological components, cells, or organs. The contamination can damage these biological systems and consequently affect the reproducibility and accuracy of these analyses. Thermal sterilization (autoclaving) is considered the most well-known technique due to its efficiency and low cost. Therefore, the ability of the fabricated epoxy resin-based chips to withstand autoclaving was assayed by applying a standard autoclaving with saturated steam at 121 °C under the pressure of approximately 15 pounds per square inch for 20 min using MaXterile 60 autoclave [16]. The autoclaving standability of the cured epoxy resin-based chips was examined by measuring their dimensions and weight before and after autoclaving accurately.

## 4 Results and discussion

### 4.1 Characterization of epoxy resin and cured epoxy resin

To the best of our knowledge, the epoxy resin may not have previously been used in bioanalysis. Therefore, characterizing the different properties of raw epoxy resin and its transparent cast chips is of importance, particularly when it was proposed to be used for fabricating a fully thermosetting epoxy microfluidic chip for POC applications as in the case

**Fig. 2** Photograph of epoxy resin-based microfluidic chip with the designed pattern composed of microchannels with (a) T-shaped, (b) straight, (c) cross, (d) lateral, and (e) Y-shaped



of this study. The findings of the characterization methods will be indicated in the following section.

#### 4.1.1 FTIR spectra

FT-IR spectra of epoxy resin and cured epoxy resin were recorded in the 400–4000 cm<sup>-1</sup> wave number range. These spectra are presented in Fig. 3. It was noticed from the spectrum of epoxy resin that the characteristic bands appeared at 823 cm<sup>-1</sup> due to the stretching vibration of C–O–C belonging to the oxirane ring. At the same time, another band that appeared at 912 cm<sup>-1</sup> is attributed to the bending vibration of CH<sub>2</sub>–O–CH of the epoxy. The band assigned to stretching C–C of the aromatic ring appeared at 1503 cm<sup>-1</sup>, whilst that assigned to stretching C=C of the aromatic ring appeared at 1601 cm<sup>-1</sup>. In addition to the bands that appeared at 2919–2857 cm<sup>-1</sup> due to stretching symmetric and asymmetric vibration C–H of CH<sub>2</sub> in aliphatic group and CH belonging to aromatic ring [17]. In the spectrum of cured epoxy resin, the band's disappearance appeared at 912 cm<sup>-1</sup> in the epoxy resin spectrum, elucidating that epoxy rings have opened. Thus, the appearance of strong broadband at 3342 cm<sup>-1</sup> attributed to –NH stretching vibrations, indicating the curing process by opening the oxirane ring and forming secondary amine. In addition to appearing an absorption band at 1108 cm<sup>-1</sup> that is typical of C–N stretching vibrations, as crosslinking progressed, the primary amine groups in the polyamine are converted to secondary and tertiary amines [18].

#### 4.1.2 Thermal stability

TGA is among the most used techniques to investigate the thermal decomposition of polymers and their thermal stability by measuring the weight loss of the material as a function of temperature. The thermal stability of cured

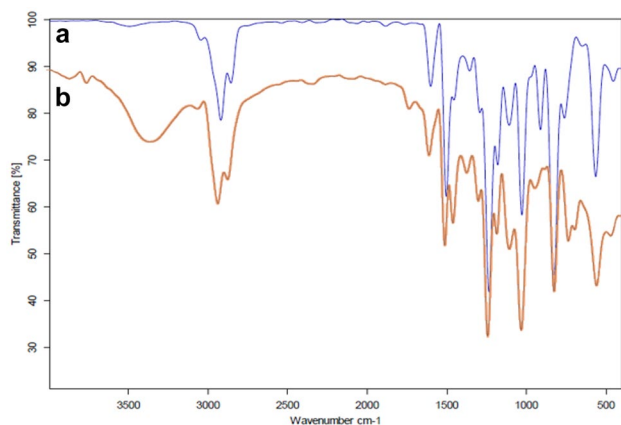
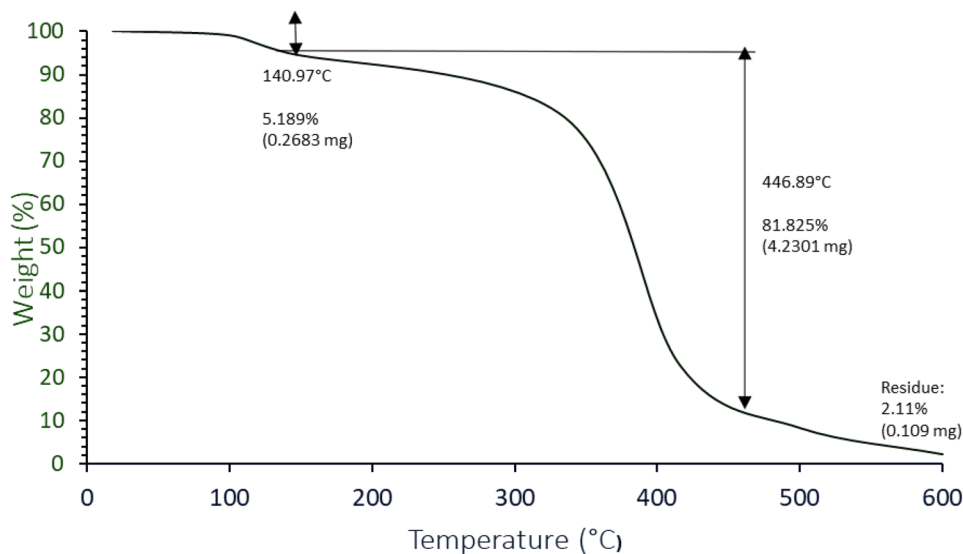


**Fig. 3** FT-IR spectra of epoxy resin (a) and cured epoxy resin (b)

epoxy resin was assessed using TGA by heating resin specimen from ambient temperature to 600 °C at a rate of 10 °C/min in a nitrogen atmosphere using TGA. The thermogram of epoxy resin is shown in Fig. 4. It was noticed from this thermogram that the thermal degradation profile of epoxy resin exhibited a three-step degradation behaviour. In the first stage, up to 140 °C, minor weight loss of epoxy resin occurred due to the evaporation of moisture and removal of air bubbles present. The second stage of degradation, in the temperature range of 140–335 °C, can be due to the homolytic scission of chemical bonds in the resin network, which influences the physical properties but does not cause a large weight loss. The third stage, considered the major stage of degradation, occurred in the temperature range between 335 and 426 °C. Derivative peak temperature ( $T_{max}$ ) and half weight loss temperature ( $T_{50}$ ) were found at 362 and 377 °C, respectively. This major weight loss can be attributed to both oxidative, and non-oxidative degradation of cured epoxies is caused by

**Fig. 4** TGA thermogram of cured epoxy resin



dehydration due to the elimination of water molecules from the oxypropylene group,  $-\text{CH}_2-\text{CH}(\text{OH})-$ , and the subsequent formation of double bonds. This dehydration is concurrent with network breakdown. The final degradation proceeds through reactions of isomerization, intramolecular cyclization, chain transfer, and other reactions involving the radicals formed in the initial stages of degradation. Finally, complete thermal decomposition occurred at  $\sim 600$  °C. In this context, it is worthy of mentioning that the laser ablation technique may raise the temperature of the treated substrate to a maximum of 150 °C, as reported extensively in many of the previous studies [19, 20]. Hence, the cured epoxy resin is considered thermally stable and suitable for microfluidic chip applications.

#### 4.1.3 Overall and specific migration

Regarding the intended application of these epoxy-based chips, it was worthy of determining the overall and specific migration because of the potential interfering and inhibition effect of the migrants on the biological assay. Therefore, the overall migration was determined by the gravimetric method; however, the specific migration was traced by gas chromatography-mass spectrometry (GC-MS) for qualitative and quantitative analyses of the migrants, including unreacted monomers and oligomers mainly that may transfer from an epoxy microfluidic chip into PCR solution. Because of the polarity of PCR solutions and being the denaturation temperature of the PCR technique of 95 °C, migration trials have been conducted using the distilled water as a simulant at 100 °C [21]. The finding of these experiments indicated that the overall migration of the cured epoxy resin prepared in this study was less than 0.1 mg/dm<sup>2</sup> of cured epoxy. The chromatogram of GC-MS is shown in Fig. 5. The chromatogram of simulant of cured epoxy resin assay (Fig. 5a) has

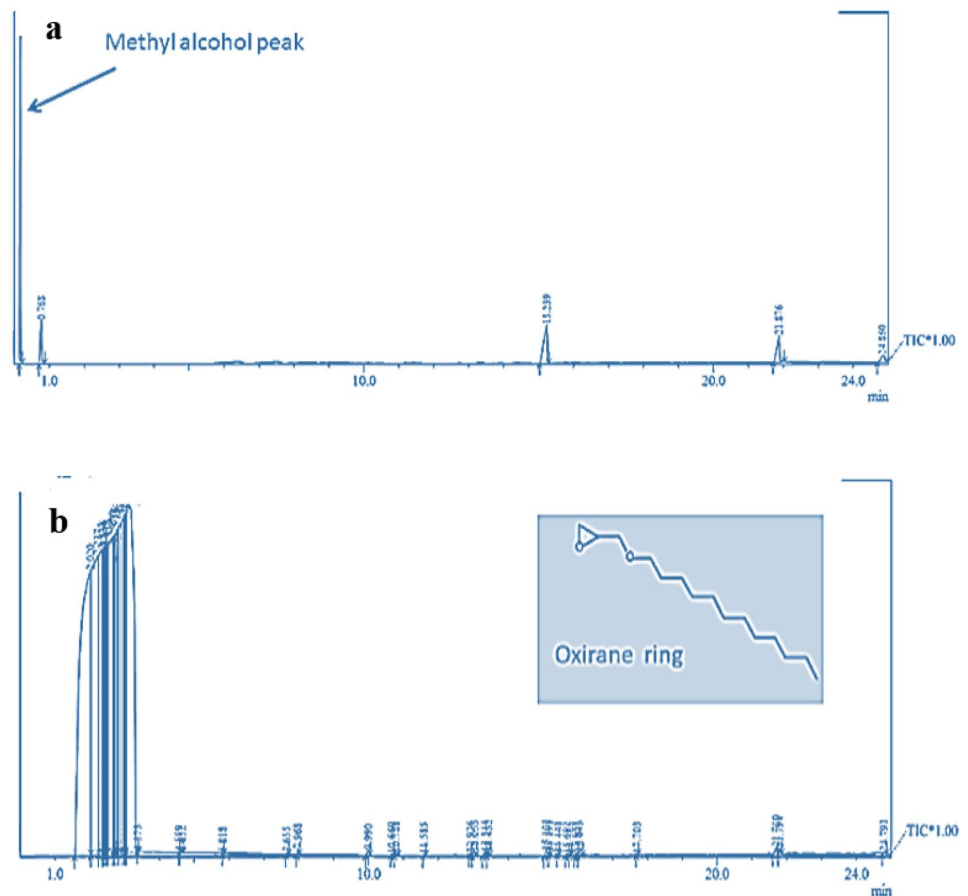
just revealed one peak that refers to the solvent, indicating no other substances have transferred from the cured epoxy resin. No detection of the migrants in the polar simulant utilized in the cured epoxy resin assay enables us to employ epoxy resin-based chips in DNA amplification and other biomedical lab-on-a-chip applications. On the other side, the potential migration of cured epoxy resin was measured with less polar simulant dichloromethane (DCM). This simulant exhibited higher potency for migration than the polar one (distilled water), where the overall migration reached  $5.3 \text{ mg/dm}^2$  of cured epoxy resin. The migration was dominated by hydrolysis products of bisphenol A diglycidyl ether (BADGE) that can be classified according to its toxicological relevance into substances regulated by the Scientific Committee of Foods (SCF) and 2002/16 EC as derivatives containing one oxirane ring (1 EPO) as indicated from the GC–MS chromatogram (Fig. 5b).

#### 4.1.4 Autoclaving endurance

In most biological applications, devices, and tools, sterilization is a crucial pre-treatment step to avoid contamination [22]. In the case of lab-on-a-chip applications, the sterilization of chips is the most common critical problem, particularly for cell culture chips and organs-on-chips, to avoid

any contamination for the analysis components [23]. In vitro cell culture can create physiologically realistic microenvironments, allowing the emergence of cell and special sterilization techniques are a must for tissue culture-based microfluidic systems. Sterilization of microfluidic chips is an integral part of the fabrication process before being used in biomedical applications by customers [24]. There are numerous sterilization processes, including the chemical (via antimicrobial agents such as ethylene oxide and hydrogen peroxide) and physico-chemical or hybrid techniques (hydrogen peroxide plasma). Nevertheless, these methods have critical drawbacks, such as the toxicity and health risks of the chemical agents and the sterilization period is lengthy. In addition to the potential negative impact of the residues of these reagents or physical processes (like plasma) on the sterilized material's chemistry and subsequently the performance of the sterilized microfluidics as another thorny drawback [25, 26]. On the other hand, autoclaving (steam sterilization under pressure) is still the most prominent due to its efficiency, ease and low cost of the process, and no use of toxic compounds [27]. Herein, the cured epoxy resin-based chips fabricated in this study were sterilized using steam sterilization (autoclave) at  $121 \text{ }^\circ\text{C}$  for 20 min under 2 atm pressure. Afterwards, the weight, dimensions, and surface roughness of the fabricated microchips were accurately

**Fig. 5** GC–MS chromatograms of migrants in different simulants. Distilled water (a). Dichloromethane (b)



measured to assess the serviceability of these chips at the autoclaving conditions. The data of these trails are tabulated in Table 2. These findings showed no significant difference in both weight and dimensions of cured epoxy resin-based chips; however, a slight decline was noticed in their surface roughness due to thermal sterilization under autoclaving conditions. Moreover, the change in width and depth and the roughness of microchannels engraved onto these chips were also examined after autoclaving. The results are listed in Table 3. So, no significant differences were observed in these parameters. On the other side, the three-dimensional laser and optical microscope micrographs of these chips after autoclaving are presented in Fig. 6. These micrographs exhibited flattening and trimming the microchip surface, making it more even by stretching irregular segments or removing unwanted melted and resolidified parts (bulges) that spread around the ablation zone by an act of steam, heat, and pressure of this process. Besides, a reduction in the height of the bulges formed on the trench rim was noticed from 3D laser microscope micrographs (Fig. 6C). Hence, this proves that cured epoxy resin-based chips have good thermo-mechanical endurance and serviceability under autoclaving conditions. Besides, the autoclaving process has a significant effect on getting ride the bulges formed around the grooves through the micromachining.

## 4.2 Optimization of CO<sub>2</sub> laser ablation system

CO<sub>2</sub> laser processing involves a few fundamental input parameters such as laser power, scanning speed, and pulse frequency can greatly influence the output microchannel dimensions, profiles, and heat-affected zone (HAZ) that affect microfluidic chip performance and efficiency. To the best of our knowledge, no previous studies have been performed to explain the effects of these parameters on resulting microchannel profiles engraved onto thermoset epoxy resin-based chips. Therefore, such laser microchanneling process was applied to draw the designed pattern on the epoxy resin-based chips at varying laser power and scanning speed to optimize such parameters, which offer the best microchannel quality and microfluidic chips performance.

**Table 2** The dimensions and surface roughness of the cured epoxy resin-based chips before and after autoclaving

Parameter	Before autoclaving	After autoclaving
Weight (gm)	2.2631	2.2631
Length (cm)	3.5	3.5
Width (cm)	3.5	3.5
Thickness (mm)	22	22
Ra (μm)	1.337 ± 0.388	1.182 ± 0.068

**Table 3** The dimensions and roughness of and CO<sub>2</sub> laser-engraved microchannel on the cured epoxy resin-based chips before and after autoclaving

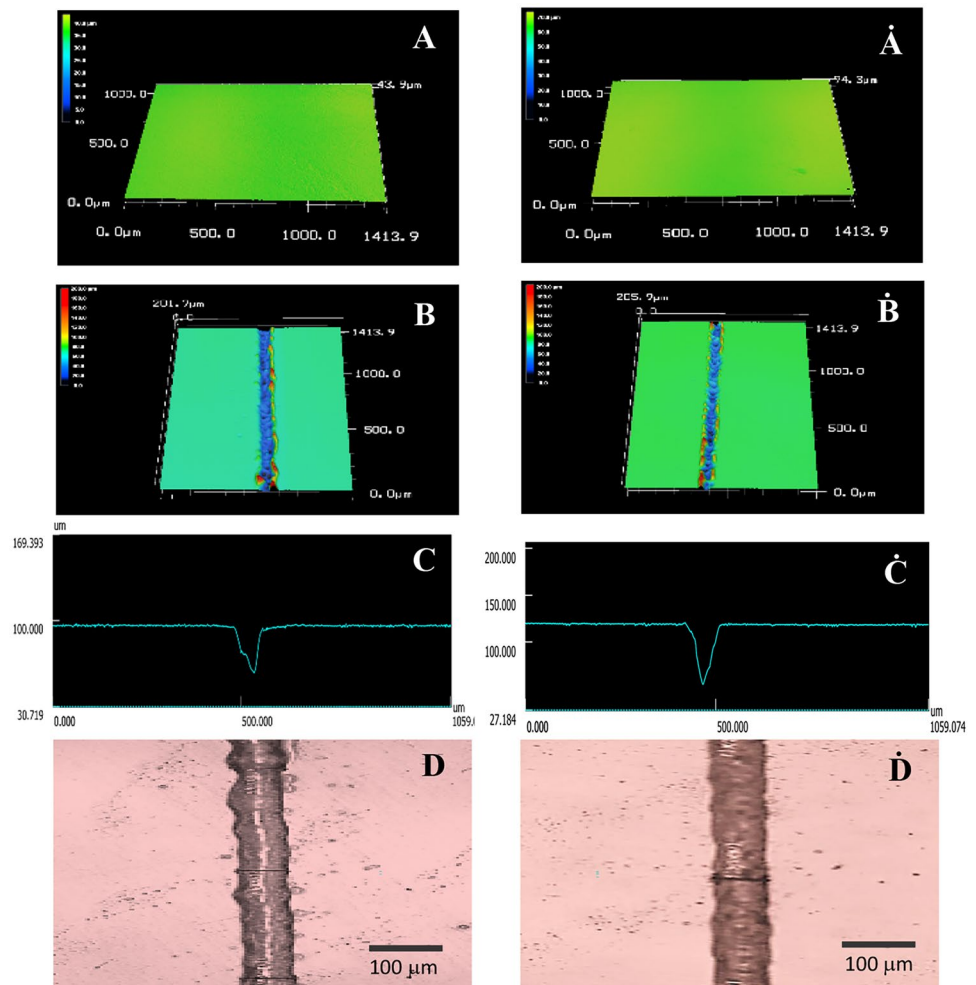
Parameter	Before autoclaving	After autoclaving
Width (μm)	91.248 ± 4.3528	98.233 ± 4.0434
Depth (μm)	48.771 ± 2.4036	48.905 ± 3.4578
Ra (μm)	8.773 ± 2.4543	7.762 ± 1.3042

### 4.2.1 Microchannel width

The impact of micromachining conditions on the microchannel width is presented in Fig. 7A. As illustrated from these findings, the width of microchannel CO<sub>2</sub> laser-ablated on thermoset epoxy resin-based chips increased with increasing laser power. Meanwhile, it was decreased with increasing the scanning speed up to 20 mm/s. These results agree with those previously reported by Prakash and Kumar for thermoplastic polymethyl methacrylate (PMMA)-based microchips [28]. Thus, the highest microchannel width ~ 165.9 μm was recorded at a scanning speed of 5 mm/s and laser power of 5.4 W. However, a noticeable increase in the trench width at a scanning speed of 15 mm/s. Afterwards, at faster-moving laser beam (> 20 mm/s), this trend was turned over, where the width of microchannel still was increased with increasing the laser power, but it was also increased with increasing the laser speed from 20 mm/s up to 30 mm/s and remain almost constant at higher speed (40 mm/s). The combination of high output power with low moving speed, as in case 5.4 W and 5 mm/s, exhibited the highest microchannel width. Therefore, the composed parameter, laser output power over moving speed (P/U), may prove a more significant effect on microchannel width than direct parameters. This relation between P/U and channel width was plotted and presented in Fig. 7B. From these findings, it can be found that this relationship passed by two stages, the first stage involving P/U from 0.05–0.18 and the second one in a range of 0.2–1.08. In the first stage, it was noticed that there is a significant difference in the width of the microchannel engraved by laser at the same P/U, where, at P/U = 0.11 in case of laser inputs, 1.8 W, 17 mm/s and 4.2 W, 40 mm/s, the width of the resulting channel was ~ 53 and ~ 108 μm, respectively. And thus, at P/U of 0.18 at laser inputs, 1.8 W, 10 mm/s and 5.4 W, 30 mm/s, the microchannel width was ~ 62 and ~ 148 μm, respectively. This indicated that the laser energy has a more pronounced effect on the microchannel width than the energy deposited onto the irradiated epoxy resin surface.

On the contrary, in the second stage, the microchanneling process that has been accomplished at the different laser input having the same P/U led to channels having comparable widths, for example, laser inputs having the same P/U

**Fig. 6** 3D laser microscope micrographs of cured epoxy resin-based chips before (A) and after autoclaving (Ā), 3D micrographs and profile of microchannel engraved at a laser power of 1.8 W and speed of 5 mm/s before (B and C, respectively) and after autoclaving (ĔB and ĔC, respectively), and optical microscope micrograph of the same microchannel before (D) and after autoclaving (ĔD)



such as 3.6 W, 15 mm/s and 4.8 W, 20 mm/s ( $P/U=0.24$ ) and 2.4 W, 5 mm/s and 4.8 W, 10 mm/s ( $P/U=0.6$ ) resulting widths ( $\sim 65$  and  $\sim 71$ ) and ( $\sim 101$  and  $\sim 106$ ), respectively. So, it was observed that the width of the trench increases as the ratio of  $P/U$  increases. It can be concluded that the microchannel width was directly proportional to the ratio of output power and moving speed. Using  $P/U$  in the range of 0.6–1 as the laser fabrication conditions will increase the absorbed energy of the material, making the fabrication easy. The channel fabricated when  $P/U$  is 0.6 is wider than the channel fabricated when  $P/U$  is 0.24. So, to fabricate microchannels with the same width, less time can be consumed, achieving more fabrication numbers at a higher value of  $P/U$ .

As well known, increasing the laser power and decreasing the scanning speed results in increasing the energy deposition on the surface of irradiated material. Simultaneously, the beam spot diameter increases with energy deposition by the laser beam in the microchanneling process. Therefore, the direct relationship between  $P/U$  and microchannel width (second stage) can be explained on the basis that the beam spot diameter increases with an increase in beam power and

decreases with an increase in scanning speed. However, the basic reason for increasing or decreasing actual beam spot diameter lies in its Gaussian distribution and threshold ablation density [29]. Assumingly, the microchannel width is equal to the actual beam spot diameter in laser micromachining. As a result, the microchannel width was directly associated with actual beam spot diameter [30]. Meanwhile, the first stage of this relationship which characterized by affecting the microchannel width more pronounced by the input power than the  $P/U$  ratio, where, by the microchanneling achieved at the same  $P/U$  ratios, higher input laser power and faster-moving speed resulted in wider channels than that at lower power and slower moving speed. These results can be attributed to the dynamic post-curing of epoxy resin, which can be taken either by the thermal effect of laser irradiation or photo-curing. As a result, post-curing, a denser network structure can be formed via photo-initiated ring-opening, reorganization and degradation reactions. Such structural modification can enhance heat transfer along the molecular chains. Such anisotropic heat transfer ability for polymer can accelerate the melting and vaporization of surficial layers of



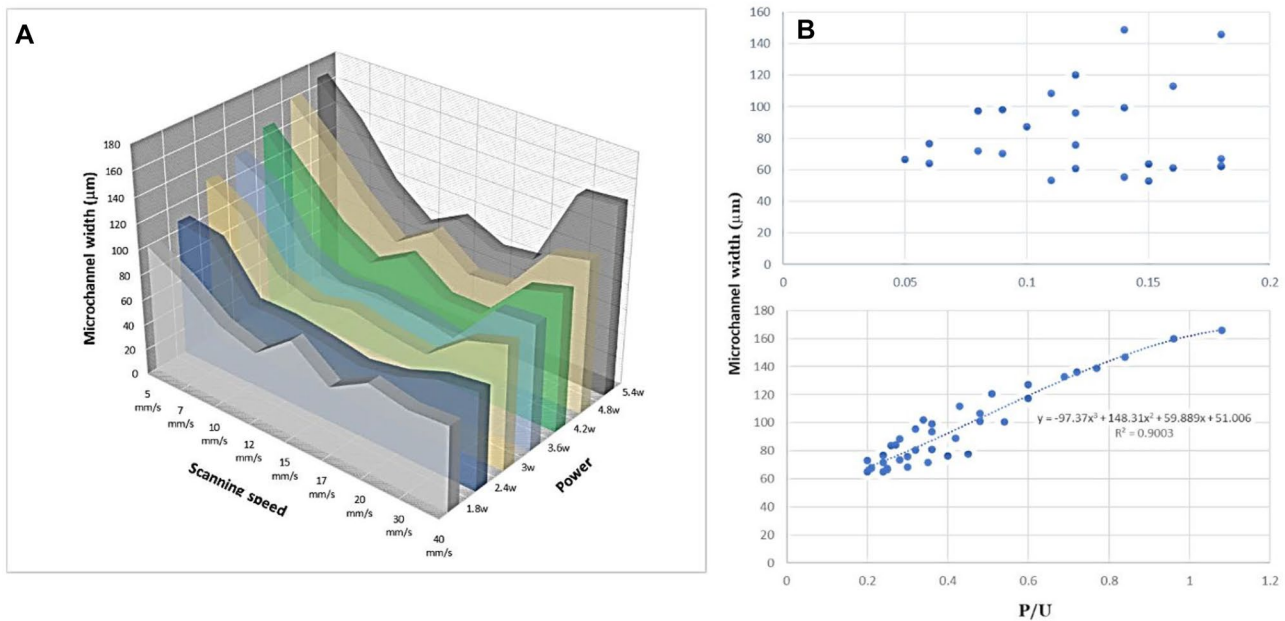


**Fig. 7** Effect of P, U (A) and P/U (B) on the width of CO<sub>2</sub> laser-ablated microchannels

epoxy resin. This can be the likely reason for increasing the microchannel width at a moving speed of 15 mm/s through the microchanneling process. Regarding the high absorptivity of epoxy resin for laser irradiation, photo-curing may play an essential role in the ablation mechanism of epoxy resin. Since the variations of thermal diffusivity and enthalpy of vaporization with temperature are negligible, the thickness of the molten layer and the recoil pressure depends mainly on the absorbed irradiance [29]. This can be confirmed by the noticeable decrease in the microchannel width resulting from laser processing at varied input power and 17 mm/s. This result proves the predominance of the photo-curing as a result of the time-dependent behaviour of irradiation. Furthermore, it was hypothesized that these photo-initiated curing reactions might occur at a certain energy threshold regardless of the irradiation intensity. As has been previously reported, promoting the ring-opening and reacting epoxide groups in epoxy resin via the activated chain end (ACE) or active monomer (AM) propagation mechanisms participates in the photo-curing process. So, a higher crosslinking density can be occurred resulting in the change of material from rubbery to the glassy state [29]. However, this tight structure implies some drawbacks, such as relative brittleness, which confers low impact resistance and the shrinkage that undergoes during the curing process (low microchannel width). On the other side, such vitrification is a physical phenomenon with reversible characteristics, where an increase of the temperature during the laser processing leads to devitrification via reorganization, cyclization and/or degradation reactions that can be induced by the thermal effect of laser

irradiation. This devitrification can lead to the gelation of epoxy resin [31]. This gelation is a chemical feature, non-reversible, which implies that the material, after reaching this point, can be subjected to more thermal degradation and vaporization and consequently increasing the microchannel width through the microchanneling process at higher power input with less pronounced effect for moving speed.

#### 4.2.2 Microchannel depth

The effect of laser input parameters on the microchannel depth is shown in Fig. 8A. It was indicated that the depth of the microchannel was increased by increasing laser power, to a certain level based on the scanning speed up to a speed of 20 mm/s. Then, it was decreased with greater power, but at faster moving speed, it increased at all applied output power. On the other side, at input power < 3.6 W, the microchannel depth was increased with increasing the scanning speed with a noticeable decrease at moving speed of 15 mm/s and relative increase at a speed of 17 mm/s. However, at greater power (> 3.6), this increase in microchannel depth was continued at faster moving speeds. The largest microchannel depth (133.4 μm) was obtained at laser power 5.4 W and scanning speed of 40 mm/s. Meanwhile, the lowest microchannel depth of about 6 μm was recorded at 4.8 W and 15 mm/s. This relationship between P/U and channel depth was plotted and shown in Fig. 8B. From these data, this relationship passed by two stages, the first stage involving P/U from 0.05–0.6 and the second one in the range of 0.6–1.08. Where it was indicated that the microchannel width was

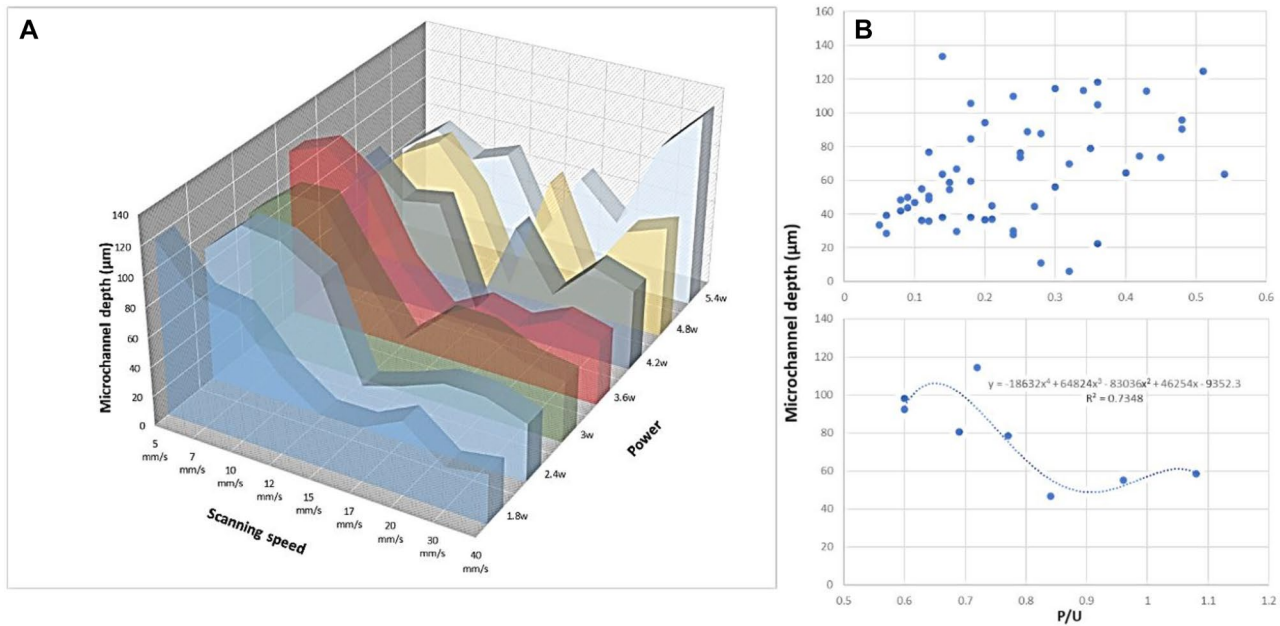


**Fig. 8** Effect of P, U (A) and P/U (B) on the depth of CO<sub>2</sub> laser-ablated microchannels

generally increasing with increasing the P/U ratio up to 0.6 with high fluctuations, Notwithstanding, it was decreased at higher ratios. Noticeably, the first stage involved the microchips that have been processed at all applied input power and most of the high moving speeds, including speeds of 15 and 17 mm/s. On the contrary, for the microchannel width results, the first scanning speed (15 mm/s) exhibited the significant decline in the values of microchannel depth. However, the latter speed (17 mm/s) led to a significant increase in these values. As the aforementioned, the high fluctuation observed in the depth of microchannel engraved at different input parameters can be attributed to the synchronization of the alteration of chemical, rheological and thermal properties of epoxy resin systems (phase-transition) and behaviour of the dominant affecting energy source (thermal and non-thermal effect) resulting in various ablation mechanisms. This can be clearly illustrated from the change in the microchannel depth engraved at different input powers at moving speeds of 15 and 17 mm/s that are associated with the phase transition, where, in the first case, the reduction in the value of depth can be attributed to that the ablation can be accomplished by a layering technique in which the laser pulse melts a thin layer of epoxy resin which evaporates so that pressure builds up and the layers are taken off the surface with generating the groove. Considering that the melting temperature of the epoxy resin was decreased because the aforementioned photo-initiated reorganization was occurring in this stage of laser ablation, acquiring an increase of heat transfer with increasing the thickness of the molten layer. This behaviour, together with the fact that the molten layer formed in the interaction

zone shield the incoming irradiation, produce a diminution in the effective irradiance, i.e. a decrease of the adsorptive infrared flux and therefore in the recoil pressure, resulting in a decrease of the groove depth. However, the increase in microchannel depth using micromachining at a scanning speed of 17 mm/s can be attributed to light/material interactions causing vitrification of epoxy resin matrix. The post-curing process, in this case, can result in a high degree of crosslinking and, therefore, modulation the rheological characteristics of the molten layer with increasing the rate of anisotropic shrinkage, causing an increase of groove depth. On the other hand, the decline in the microchannel depth with increasing the P/U ratios at values higher than 0.6 can be attributed to insufficient time to transfer the heat energy within the polymer lattice at higher speed, causing minimal thermal damage and consequently generating the trench with lower depth [30]. In this context, it is worth mentioning that scorch, and yellowish colour began to appear at high input power and low scanning speed. Due to the presence of aromatic ring structures in epoxy resins that can absorb light, they are easily oxidized to form carbonyl groups forming chromophores when they absorb ultraviolet rays or heating. This discolouration, which in turn leads to a decrease in the transmittance of the epoxy resin, can affect the microfluidic efficiency via hindering viewing the fluids during their flow within the microchannels.

#### 4.2.3 Aspect ratio

The aspect ratio is a dividing product of microchannel depth by microchannel width. A high aspect ratio of a

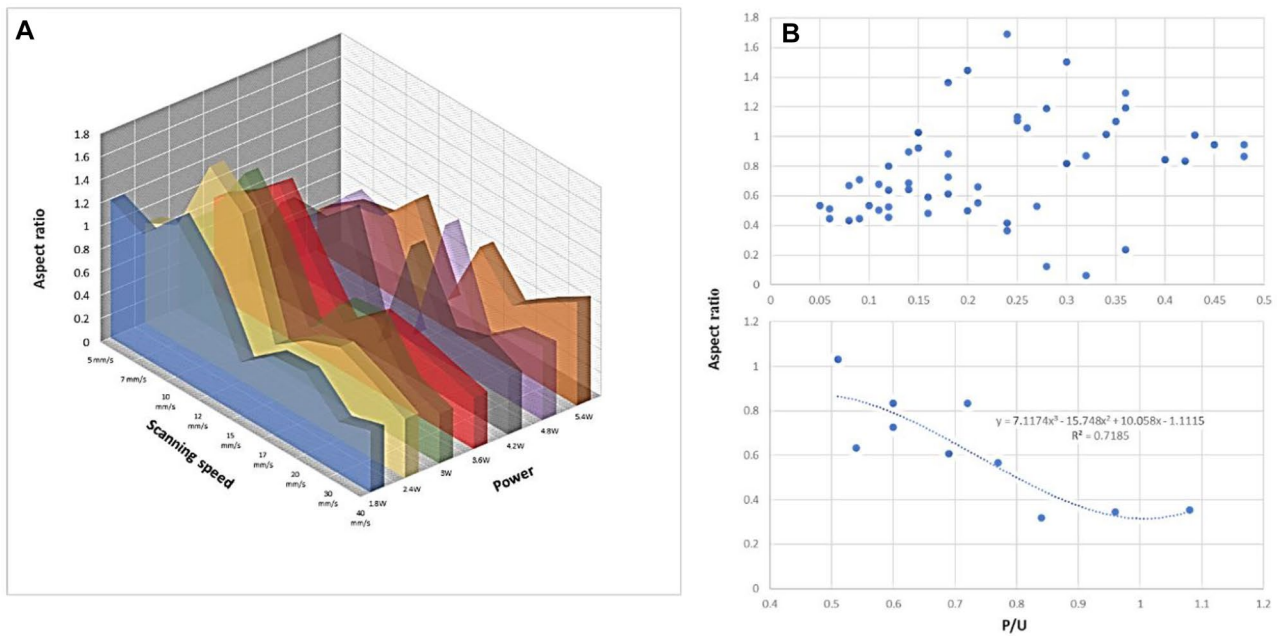


**Fig. 9** Effect of P, U (A) and P/U (B) on the aspect ratio of CO<sub>2</sub> laser-ablated microchannels

microchannel is recommended in the application of microfluidic chips, particularly in life science, to allow the combination of cell screening action and high fluidic throughput in continuous flow systems [29]. The impact of input power and scanning speed on the aspect ratio was presented in Fig. 9A. It was observed from these findings that the aspect ratio was decreased with increasing the laser power up to 3.6 W with increment in the decrease rate at higher power. This trend kept up to a scanning speed of 15 mm/s. However, the aspect ratio increased by increasing the input power up to 4.8 W or 3 W and decreased at higher power at moving speeds of 17 and 20 mm/s, respectively. Thus, at a scanning speed of 30 mm/s, this ratio was increased with increasing the input power up to 2.4 W and remain almost constant at higher power, whilst, at 40 mm/s, it was decreased with increasing the input power up to 3.6 W and remained almost constant at higher power. On the other side, the aspect ratio was increased by increasing the scanning speed from up to 10 or 12 mm/s based on the input power. But the higher speeds were accompanied by a decline in the aspect ratio with a significant decrease at scanning speed at 15 mm/s followed by a relative increase in faster-moving speed of at 17 mm/s. This relative increase was highly significant at input power > 3.6 W. The maximum aspect ratio (1.691) was recorded at a power of 2.4 W and a scanning speed of 10 mm/s. However, the lowest aspect ratio (0.063) was exhibited at 4.8 W and scanning speed of 15 mm/s. Thus, the relationship between P/U and aspect ratio is shown in Fig. 9B. From these data, this relationship passed by two

stages, the first stage involving P/U from 0.05–0.48 and the second one in the range of 0.48–1.08, where it was indicated that the aspect ratio was generally increasing with increasing the P/U ratio up to 0.48 with high fluctuations. Notwithstanding, it was decreased at higher ratios. These data can also be interpreted from the discussion of the datum mentioned above of microchannel width and depth.

#### 4.2.4 Microchannel quality

In addition to the dimensional stability, surface roughness and bulge heights are considered essential determinants of the quality of the microchannel of microfluidic chips used in LOC applications. In this context, despite the special significance of laser ablation technique for the manufacturing of polymers-based microfluidic platforms, the engraved areas of the manufactured devices have relatively bulky surface roughness, which disrupts smooth fluidic flow and damages sensitive biological components [11]. Furthermore, the thermal effect of laser beams on the polymeric substrate through micromachining can cause some heat defects such as bulges forming parallel along the microchannels or, in some cases, splashes. Besides, heat-affected zone (HAZ) around the rim of microchannels and holes. These bulges may impact the bonding efficiency or even clog the channels [31–34]. To study the effect of different input parameters on the geometry and quality of microchannel, a three-dimension laser scanning microscope (Keyence VK-X100) was used to obtain the 3D topography of the microchannel (3D profile measurements).

**Microchannel roughness** The surface roughness of microchannels is an essential criterion for many microfluidics applications. The arithmetic average of roughness ( $R_a$ ), which is the average arithmetic height of surface irregularities (peaks and valleys) from the mean line along the scanning length in the bottom of the microchannel, was adopted as a measure of surface roughness [24]. The impact of input power and scanning speed on the surface roughness of the microchannel was depicted in Fig. 10A. Similarly, as in the case of microchannel dimensions, it was indicated that an astonishing diversity of the relationship between the input power and roughness based on the scanning speed where their curves have polynomial functions with different degrees. In general, the roughness of the microchannel was decreased with increasing the input power with a noticeable relative increase at power greater than 3.6 W in case of the fastest moving speed (40 mm/s). On the other side, the roughness was reduced with rising the moving speed with a noticeable reduction at a scanning speed of 15 mm/s and a relative increase at a speed of 17 mm/s as well as at 30 mm/s with input power of 5.4 W and 30 mm/s with input power of 4.2–4.8 W. The highest roughness ( $\leq 36 \mu\text{m}$ ) was achieved from laser processing at a high laser power of 5.4 W and a high scanning speed of 30 mm/s. However, the lowest roughness ( $\leq 3 \mu\text{m}$ ) was achieved at a high laser power of 4.8 W and a high scanning speed of 15 mm/s.

By considering the effect of the composed parameter, P/U, on the roughness shown in Fig. 10B, it was illustrated that the roughness of the microchannel was increased by increasing the P/U ratio up to 0.84, whilst it decreased at higher ratios. This polynomial correlation involved three stages, the first stage involving P/U from 0.05–0.24, in which the roughness parameter was increased with increasing the

P/U with comparable values for the microchanneling accomplished at the same P/U ratio either by combination higher input power and slower scanning speeds or lower power with faster speed. Notwithstanding, in the second stage at the P/U ratio from 2.4 to 0.84, the roughness was also increased with increasing the P/U at a lower rate. Besides, the roughness value obtained at the same P/U ratio in the range of 0.24 to 4.8 was much different as a result of including the laser processing at the scanning speed of 15 and 17 mm/s at which the roughness was in the domain of variations of epoxy resin surface irregularities with a significant decrease or increase in the roughness values, respectively. In the third stage in the range of 0.084–1.08, the microchannel roughness was noticeably decreasing with increasing the P/U ratio.

The decrease of surface roughness with increasing the input power and decreasing the scanning speed throughout the micromachining can be explained based on increasing the temperature that accelerates the kinetics of melting and vaporization processes with minimization of the plume etching resulting from plume confinement with a pulsed laser beam at fluences over the ablation threshold [35]. This can also be the likely reason for the significant decrease in the surface roughness during micromachining at a moving speed of 15 mm/s. As stated above, the post-curing reactions that can be occurred in this stage can lead to a decrease in the viscosity of the molten layer which allows expanding the ablation plume. On the contrary of faster moving speed (17 mm/s), the vitrification of epoxy resin matrix occurred in this stage is associated with increase the crosslinking density, and therefore, the plume confinement was increased to cause higher surface etching [34]. In this respect, it is worth to state the noticeable reduction in the surface roughness for microchannel machined at varying input power and scanning speed of 20 mm/s can be attributed to gelation of epoxy

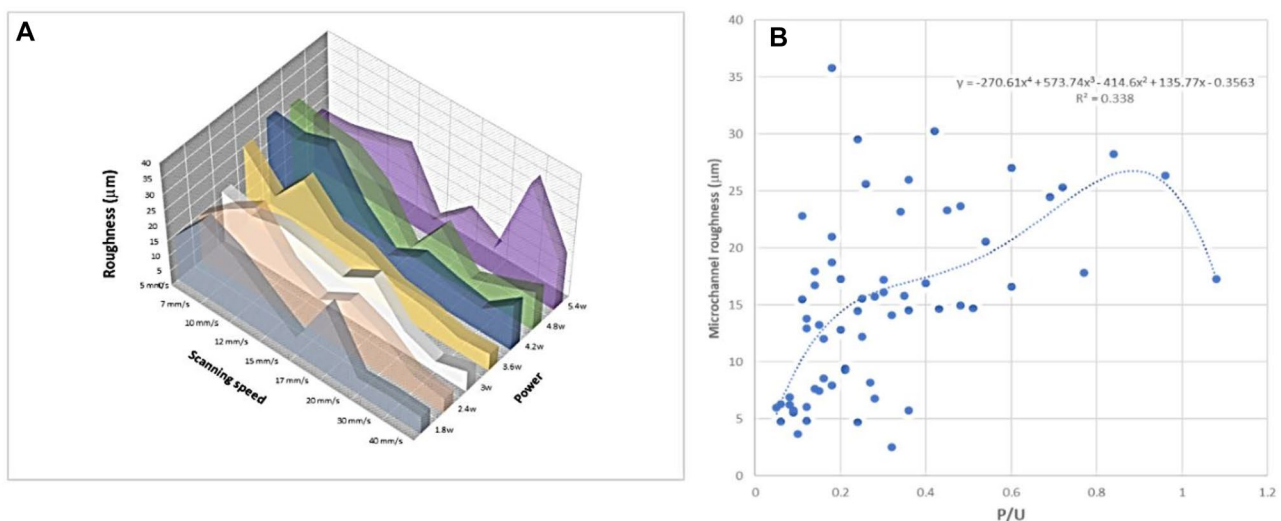


**Fig. 10** Effect of P, U (A) and P/U (B) on the roughness of  $\text{CO}_2$  laser-ablated microchannels

resin at this micromachining parameter causing vicinity and fusion molten bulges resulting in a dummy uniformity. This may show that these surfaces had less irregularities, i.e., lower roughness, as in Fig. 10.

**Bulge height** The relationship between laser fabrication parameters and the height of the bulge was established. The results are shown in Fig. 11A. From these data, it was noticeable that this relationship was highly comparable for its corresponding laser processing parameters with surface roughness. It was illustrated that the height of the bulge was also decreased with increasing the input power with a noticeable relative increase at power greater than 3 W in case of the fastest moving speed (40 mm/s). Meanwhile, the bulge height was declined with accelerating the laser scanning with a noticeable reduction at a scanning speed of 15 mm/s and relative increase at a speed of 17 mm/s and at 30 mm/s with input power 5.4 W and 30 mm/s with input power of 3.6–4.8 W. The maximum bulge height (> 140  $\mu\text{m}$ ) was recorded at an input power of 4.2 W and scanning speed of 5 mm/s. However, the lowest bulge height ( $\sim 20$  nm) exhibited when micromachining was achieved at 1.8 W and 5 mm/s. On the other side, the effect of the composed parameter, P/U, on the bulge height was shown in Fig. 11B; it was illustrated that bulge height was increased with increasing P/U ratio up to 0.84, whilst it decreased at higher ratios. The increment in bulge height can be divided into two stages; the first stage with a P/U ratio from 0.05 to 0.6 is the domain of bulge height variation, where many different heights were recorded for laser fabrication on the same P/U as a result of including the varying heights of bulges machined on scanning speed of 15 and 17 mm/s.

It is worthy to mention here that the flowing of ablated material on the rims of the microchannel and subsequently

distortion of these rims occurs as a result of the rapid increase in the temperature of laser-projected epoxy resin. The elastomer epoxy resin consists of a hard segment, a soft segment, and a chain extender. The volume ratios, distributions and chemical compositions of each segment and the level of crosslinking influence the properties of epoxy resin. So, the phase transition in this thermoset epoxy resin is because of the motion of this soft segment (amorphous structure) of epoxy resin expanded and extruded by the thermal stress induced by great temperature gradient and resolidified by cooling with atmospheric air to form bulges. The larger deformation in the structure occurs when the temperature exceeds the threshold deformation temperature. Consequently, the number of bulges formed along the laser ablation zone on epoxy resin and their height have been ultimately increased due to an increase of the laser power and reduction of the scanning speed [34]. Thus, a decrease of the polymer binding energy because of phase transition occurring at 15 mm/s led to a lower thermal gradient with lower interfacial tension between different states within the fusion zone and surface tension, i.e. gas–liquid tension between the molten polymer material and the surrounding medium. In addition to ease release of gaseous species and therefore the decline of bulge height. On the contrary, increasing the bulge height on micromachining at a scanning speed of 17 mm/s can be attributed to increasing the binding energy of polymer by rising the crosslinking density through the vitrification phenomenon and changing the flowing state of polymer to the glassy solid state. Thus, squeezing the molten polymer layer out of the groove to form the bulges will become more difficult. Nevertheless, the higher temperature gradient in the fusion zone can lead to extrusion of the softened polymer materials near the ablation pool, forming the bulges [35]. Furthermore, the thermal state of the epoxy

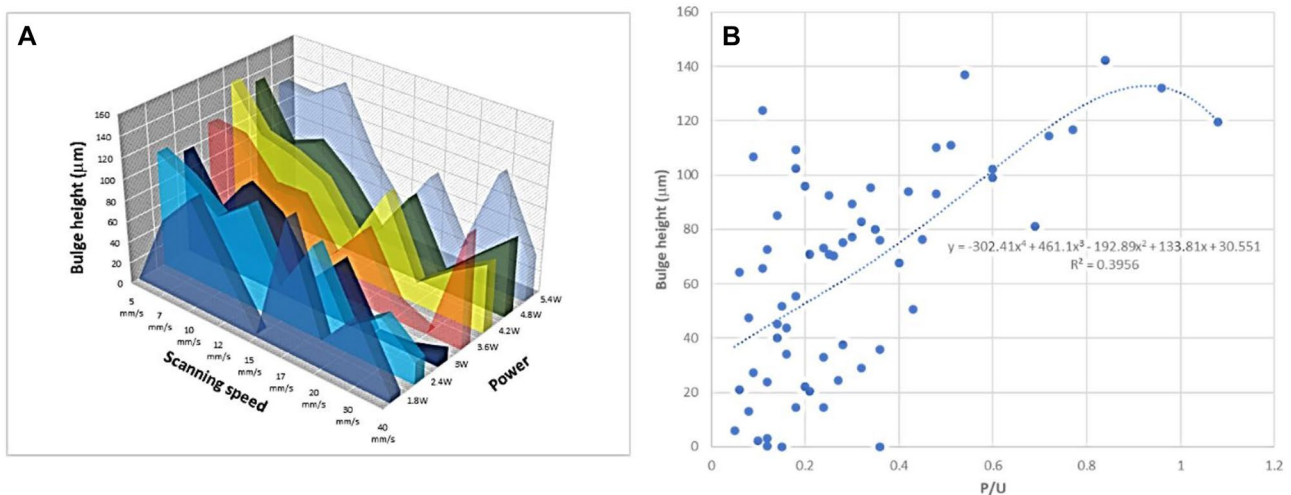


**Fig. 11** Effect of P, U (A) and P/U (B) on bulge height of  $\text{CO}_2$  laser-ablated microchannels

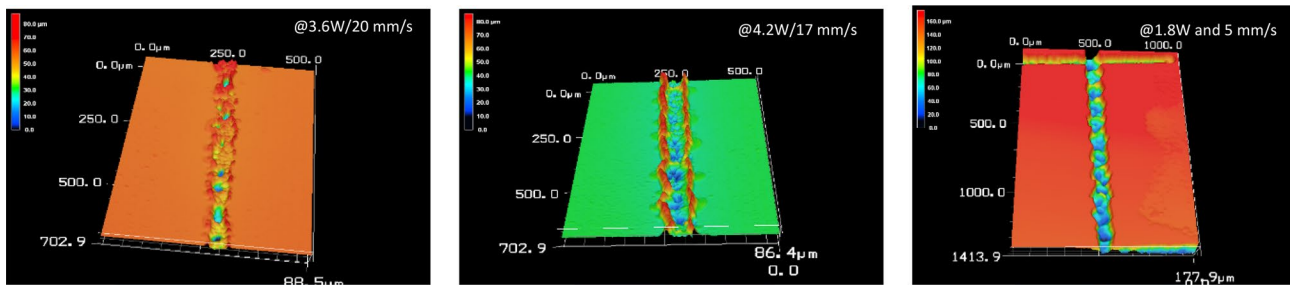


**Fig. 12** 3D profile of microchannels machined at different laser power and speed

resin workpiece is dependent on the microchannel profile along with the binding energy of the polymer and interfacial and superficial tension [34]. The formation of bulges in the rim of the microchannel machined at an input power of 4.2 and 17 mm/s and clogging in the microchannel machined at an input power of 3.6 and 20 mm/s can be shown from the three-dimension topographical micrographs (3D profiles). In the same context, the well-configured microchannel having the least bulges with the lowest height exhibited at an input power of 1.8 and 5 mm/s. These 3D micrographs were presented in Fig. 12.

**Heat-affected zone (HAZ)** The heat-affected zone (HAZ) is the unavoidably heat-treated area in the parent plastic workpiece near the fusion zone during ablation where structural transformations occur [12]. The influence of the laser processing parameters on the heat-affected zone in epoxy resin-based microchips was studied, and the results were shown in Figs. 13A, B and 14. These findings exhibited that HAZ was generally extended with raising the laser

power. Whilst, it was narrowed with accelerating the scanning speed, with a slight relative decline at moving speed of 12 and 17 mm/s and a noticeable increase at a speed of 15 mm/s. Maximum HAZ observed on these epoxy resin-based chips was less than 30  $\mu\text{m}$  when machined by laser ablation in the air at the highest input power and slowest scanning speed (5.4 W and 5 mm/s). Regarding the effect of the P/U ratio on HAZ, the results shown in Fig. 13B indicated that HAZ formed onto epoxy resin chips was increased with increasing P/U ratio. The polynomial curve indicating the relationship between two variables, HAZ and P/U passed by four stages; in the first one (P/U = 0.05–0.18), HAZ was gradually raised with increasing P/U ratio at a high rate with less noise and fluctuations. The second stage (P/U = 0.18–0.4) revealed an increase in HAZ with increasing P/U with high fluctuations for HAZ values at the same P/U ratio as a result of including the laser processing at speeds of 12, 15, and 17 mm/s. Whilst the third stage (P/U = 0.4–0.84) showed a significant increase in HAZ with increasing P/U at a lower rate compared with its corresponding in the first

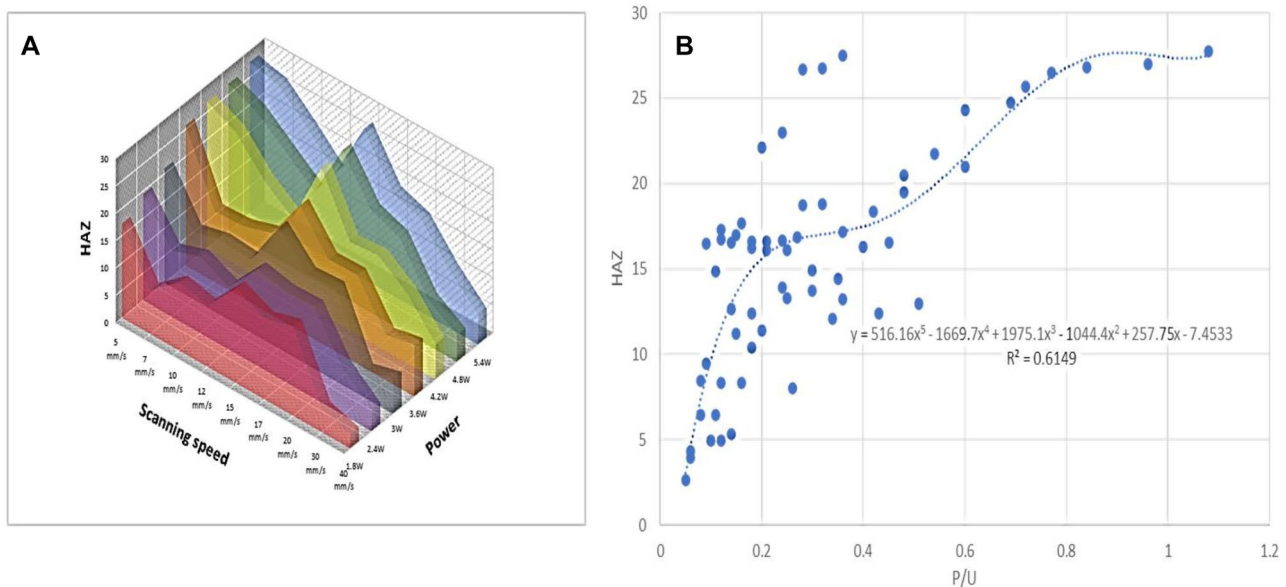


**Fig. 13** Effect of P, U (A) and P/U (B) on HAZ on epoxy resin-based microchips

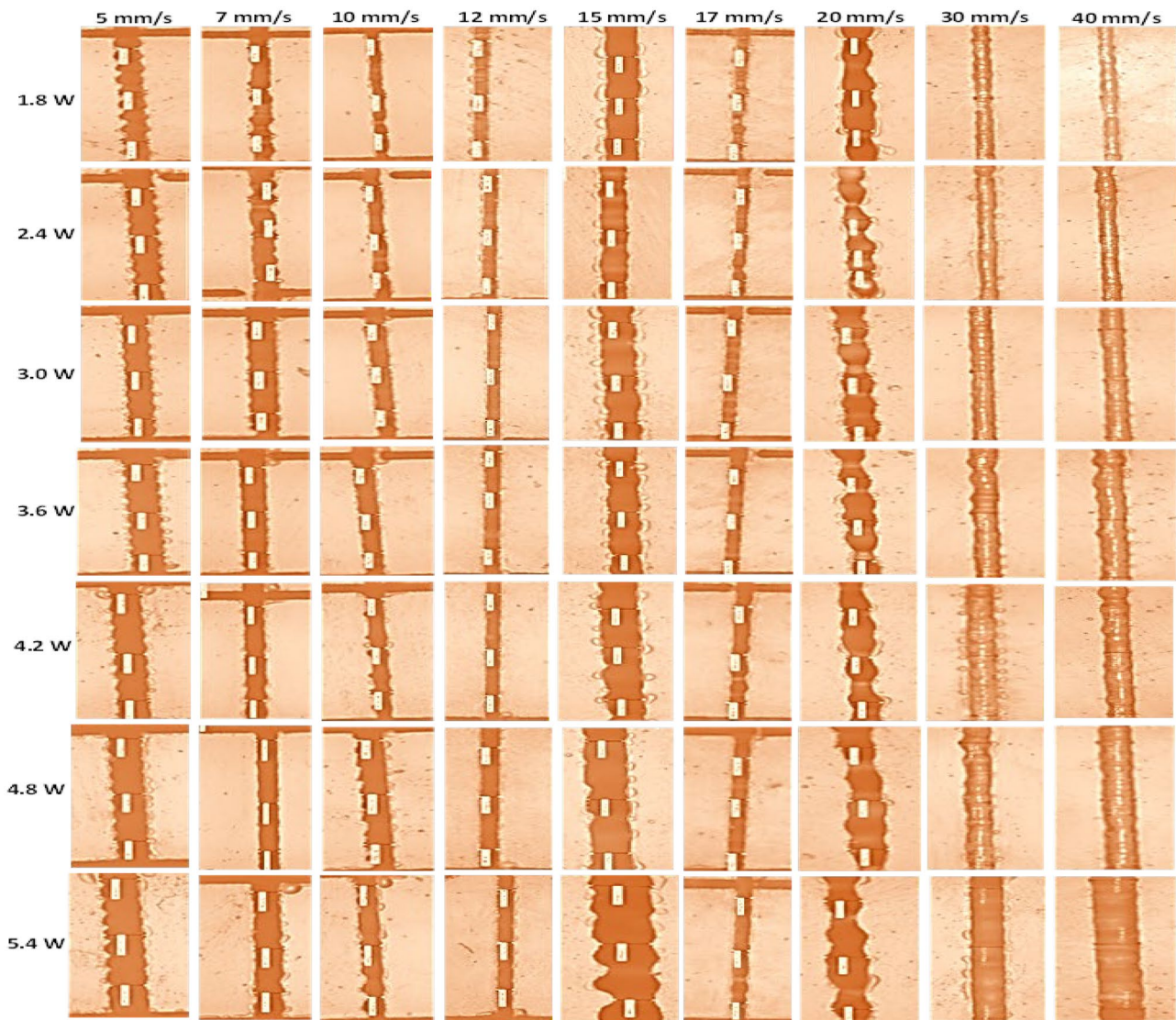


**Fig. 14** Micrographs of epoxy resin machined using CO<sub>2</sub> laser at varying laser powers and scanning speeds

stage. Finally, the HAZ remained almost constant in the later stage ( $P/U = 0.84\text{--}1.08$ ). Both of the two latter stages have less noise, where the experimental data points were highly fit with the polynomial trend.

Undoubtedly, widening HAZ with increasing the input power and decreasing the scanning speed throughout the micromachining can be explained based on increasing the temperature of the fusion zone with the accumulation of the heat laterally along the ablation zone leading to high thermal stress [35]. As a result, cracks and distortions can occur due to the expansion and contraction of the polymer melt during the ablation process. The micromachining at speeds of 12 and 17 mm/s was associated with increasing the polymer binding energy via increasing the crosslinking density. This can lead to absorbing more energy in the photo-thermal

curing process preventing its accumulation and transferring the excess outside the ablation zone. Consequently, less thermal stress occurred in HAZ. In contrast to this case, accomplishing the laser microfabrication at speeds of 15 and 20 mm/s was associated with lowering the crosslinking density of epoxy resin matrix, allowing melting and flowing the softened materials (thermal degradation and gelation), which transfer the surplus of energy to the unprocessed vicinity. This can be the potential reason for increased HAZ.

By comparing epoxy resin-based microchips fabricated in this study with PMMA, epoxy resin chips exhibited a much small heat-affected zone ( $< 30\ \mu\text{m}$ ). However, PMMA machined with laser ablation process under similar conditions showed wider HAZ either in the air or underwater, previously reported 493 and 142  $\mu\text{m}$ , respectively [33]. This can be explained on the basis that epoxy resin has an

extremely low thermal conductivity  $\kappa=0.2$  W/(m\*K) [36]. The low thermal conductivity (high thermal resistances) leads to good heat dissipation and subsequently steep thermal gradients and low thermal stress resulting in asymmetric heat-affected zones (HAZ) during ablation trials [34, 35]. In this context, the HAZ geometry may be affected by the microchannel dimensions and the cooling time [34].

## 5 Conclusions and future work

Thermosetting epoxy resin-based microfluidics has been successfully fabricated with simple, mask-less, and rapid operations, including casting and CO<sub>2</sub> laser ablation micromachining. It was found that commercially available epoxy resin has many vital properties that make it a good potential candidate for microfluidics, such as high young's modulus, hydrophobicity, high optical transparency, thermal stability, autoclavability, negligible migration, easiness of handling and low cost. Moreover, low-cost patterning and great automation throughput of laser ablation can offer industrial scalability for epoxy resin in lab-on-a-chip applications. In respect to testing out CO<sub>2</sub> laser micromachining for cured epoxy resin for the first time in this study, this process has been accomplished using laser power in a range of 1.8 to 5.4 W, and scanning speed in the range of 5 to 40 mm/s to determine the best parameters for processing cured epoxy resin. Since increasing the aspect ratio and reducing both roughness and thermal defects are essential for microfluidic performance, the findings of this study demonstrated that achieving these targets simultaneously encounters difficulty because the laser intensity required for microchanneling (high aspect ratio) can increase the surface roughness and heat defects. In this context, laser micromachining at an input power of 1.8 W and scanning speed of 5 mm/s is the compromise. The microchannel aspect ratio was about 1.19 and reasonable surface roughness (Ra) of ~15  $\mu\text{m}$ . Meanwhile, the bulge height was 0.027  $\mu\text{m}$  with no clogging, and HAZ was less than ~18  $\mu\text{m}$ . This study proves the potential feasibility of CO<sub>2</sub> laser ablation for microfabrication of cured epoxy resin-based microfluidic chips for various applications.

The physical and chemical processes occurring by the act of laser-epoxy resin interactions are in the microscale version, where they only occur in the fusion zone, which its dimensions are in micrometres. Therefore, microscale modelling methodology for mass and heat transfer in chemical reactions, phase-transition phenomena, and flow properties are highly recommended to be developed in further studies. Furthermore, innovative bio-based coatings and epoxy resin nanocomposites are suggested to improve the biocompatibility and heat resistance of microfluidics, especially in the life science field.

**Acknowledgements** The authors would like to thank the Ministry of Higher Education and Scientific Research of Egypt for the financial support of the Scholarship provided to Heba Mansour for a PhD. Thanks should be extended to Japan International Cooperation Agency (JICA) and Science and Technology Development Fund, project STDF-12417, for partially supporting this research equipment.

**Authors' contributions** A. M. Fath El-Bab and E. A. Soliman elaborated the concept of the study. Heba Mansour performed and analysed the experimental investigations with the support of the other authors. Heba Mansour wrote the manuscript in consultation with E. A. Soliman and A. Abdel-Mawgood participated in the design of the study and its coordination.

**Funding** Open access funding provided by The Science, Technology & Innovation Funding Authority (STDF) in cooperation with The Egyptian Knowledge Bank (EKB). This work is supported by the Ministry of Higher Education (MoHE) of the Egypt Government.

**Data availability** The paper has no associated software. All data gathered regarding this publication is presented.

## Declarations

**Ethics approval** All procedures performed in studies involving human participants were in accordance with the ethical standards of the institutional and/or national research committee and with the 1964 Helsinki Declaration and its later amendments or comparable ethical standards.

**Consent to participate** Informed consent was obtained from all authors who participated in the study.

**Consent for publication** The authors have consented to publish the research article in the journal.

**Conflict of interest** The authors declare no competing interests.

**Open Access** This article is licensed under a Creative Commons Attribution 4.0 International License, which permits use, sharing, adaptation, distribution and reproduction in any medium or format, as long as you give appropriate credit to the original author(s) and the source, provide a link to the Creative Commons licence, and indicate if changes were made. The images or other third party material in this article are included in the article's Creative Commons licence, unless indicated otherwise in a credit line to the material. If material is not included in the article's Creative Commons licence and your intended use is not permitted by statutory regulation or exceeds the permitted use, you will need to obtain permission directly from the copyright holder. To view a copy of this licence, visit <http://creativecommons.org/licenses/by/4.0/>.


## References

1. Cui P, Wang S (2019) Application of microfluidic chip technology in pharmaceutical analysis: a review. *J Pharm Anal* 9(4):238–247. <https://doi.org/10.1016/j.jpha.2018.12.001>
2. Niculescu AGC, Chircov A C, Grumezescu BAM (2021) Fabrication and applications of microfluidic devices: a review. *Int J Mol Sci* 22(4):1–26. <https://doi.org/10.3390/ijms22042011>
3. Chiesa E et al (2018) The microfluidic technique and the manufacturing of polysaccharide nanoparticles. <https://doi.org/10.3390/pharmaceutics10040267>



4. Whitesides GM (2006) The origins and the future of microfluidics. *Nature* 442(7101):368–373. <https://doi.org/10.1038/nature05058>
5. Fallahi H, Zhang J, Phan HP, Nguyen NT (2019) Flexible microfluidics: fundamentals, recent developments, and applications. *Micromachines* 10(12). <https://doi.org/10.3390/mi10120830>
6. Morgan NY (2021) Microfabricated devices for confocal microscopy on biological samples. In *Confocal Microscopy* 2304:93–109
7. Pan LJ et al (2018) Controllable synthesis of nanocrystals in droplet reactors. *Lab Chip* 18(1):41–56. <https://doi.org/10.1039/c7lc00800g>
8. Tsao CW (2016) Polymer microfluidics: simple, low-cost fabrication process bridging academic lab research to commercialized production. *Micromachines* 7(12). <https://doi.org/10.3390/mi7120225>
9. Fang Y, Kang H, Wang W, Liu H, Gao X (2010) Study on polyethylene glycol/epoxy resin composite as a form-stable phase change material. *Energy Convers Manag* 51(12):2757–2761. <https://doi.org/10.1016/j.enconman.2010.06.012>
10. Yuan W, Li LH, Lee WB, Chan CY (2018) Fabrication of microlens array and its application: a review. *Chinese J Mech Eng*. <https://doi.org/10.1186/s10033-018-0204-y>
11. Mohammed MI, Alam MNHZ, Kouzani A, Gibson I (2017) Fabrication of microfluidic devices: improvement of surface quality of CO<sub>2</sub> laser machined poly(methylmethacrylate) polymer. *J Micro-mech Microeng* 27(1):15021. <https://doi.org/10.1088/0960-1317/27/1/015021>
12. Cai J et al (2017) Rapid prototyping of cyclic olefin copolymer based microfluidic system with CO<sub>2</sub> laser ablation. *Microsyst Technol* 23(10):5063–5069. <https://doi.org/10.1007/s00542-017-3282-3>
13. Toossi A, Daneshm M, Sameoto D (2013) A low-cost rapid prototyping method for metal electrode fabrication using a CO<sub>2</sub> laser cutter. *J Micromech Microeng* 23(4):47001. <https://doi.org/10.1088/0960-1317/23/4/047001>
14. Han D, Yoshida K, Kim J (2020) Effective and efficient removing method of micromolds in UV-LIGA using CO<sub>2</sub> laser ablation followed by O<sub>2</sub>/CF<sub>4</sub> plasma finishing for high-aspect-ratio metallic microstructures. *Int J Adv Manuf Technol* 110:1–15. <https://doi.org/10.1007/s00170-020-06065-4>
15. Sendón R, Bustos J, Santillana MI (2019) GC-MS screening for the identification of potential migrants present in polymeric coatings of food cans
16. Yan JP (2017) Development of an epoxy-based microfluidic device for automated circulating tumour cell separation. The University of British Columbia, Vancouver. <https://doi.org/10.14288/1.0354561>
17. González MG, Cabanelas JC, Baselga J (2012) Applications of FTIR on epoxy resins – identification, monitoring the curing process, phase separation and water uptake. <https://doi.org/10.5772/36323>
18. Nolic G, Zlatkovic S, Cakic M, Cakic S, Lacnjevac C, Rajic Z (2010) Fast fourier transform IR characterization of epoxy GY systems crosslinked with aliphatic and cycloaliphatic EH polyamine adducts. *Sensors* 10(1):684–696. <https://doi.org/10.3390/s100100684>
19. Romão BMV et al (2006) Characterization of the curing agents used in epoxy resins with TG/FT-IR technique. *Polimeros* 16(2):94–98. <https://doi.org/10.1590/S0104-14282006000200007>
20. Emmelmann C, Petersen M, Goeke A, Canisius M (2011) Analysis of laser ablation of CFRP by ultra-short laser pulses with short wavelength. *Phys Procedia* 12(PART 1):565–571. <https://doi.org/10.1016/j.phpro.2011.03.071>
21. Kim J, Parkand C, Kim Y (2021) Quantitative analysis of fluorescence detection using a smartphone camera for a PCR Chip
22. Zhang R et al (2014) Microfluidic sterilization. *Biomicrofluidics* 8(3):6–10. <https://doi.org/10.1063/1.4882776>
23. Yan JP (2017) Development of an epoxy-based microfluidic device for automated circulating tumour cell separation. Dissertation, The University of British Columbia
24. Yavuz C, Oliaei SNB, Cetin B, Yesil-Celiktas O (2016) Sterilization of PMMA microfluidic chips by various techniques and investigation of material characteristics. *J Supercrit Fluids* 107:114–121. <https://doi.org/10.1016/j.supflu.2015.08.019>
25. White A Burns D, Christensen TW (2006) Effective terminal sterilization using supercritical carbon dioxide. *J Biotechnol* 123(4):504–515. <https://doi.org/10.1016/j.jbiotec.2005.12.033>
26. De Moraes MA, Weska RF, Beppu MM (2014) Effects of sterilization methods on the physical, chemical, and biological properties of silk fibroin membranes. *J Biomed Mater Res Part B Appl Biomater* 102(4):869–876. <https://doi.org/10.1002/jbm.b.33069>
27. Zhang J, Davis TA, Matthews MA, Drews MJ, LaBerge M, An YH (2006) Sterilization using high-pressure carbon dioxide. *J Supercrit Fluids* 38(3):354–372. <https://doi.org/10.1016/j.supflu.2005.05.005>
28. Prakash S, Kumar S (2018) Pulse smearing and profile generation in CO<sub>2</sub> laser micromachining on PMMA via raster scanning. *J Manuf Process* 31:116–123. <https://doi.org/10.1016/j.jmapro.2017.11.003>
29. Morancho JM, Cadenato A, Ramis X, Morell M, Fernández-Francos X, Salla JM, Serra A (2013) Unexpected differences between thermal and photoinitiated cationic curing of a diglycidyl ether of bisphenol A modified with a multiarm star poly(styrene)-b-poly(ε-caprolactone) polymer. *eXPRESS Polym Lett* 7(7):565–576. <https://doi.org/10.3144/expresspolymlett.2013.54>
30. Snakenborg D, Klank H, Kutter JP (2004) Microstructure fabrication with a CO<sub>2</sub> laser system. *J Micromechanics Microengineering* 14(2):182–189. <https://doi.org/10.1088/0960-1317/14/2/003>
31. Foix D, Ramis X, Serraand A, Sangermano M (2011) UV generation of a multifunctional hyperbranched thermal crosslinker to cure epoxy resins. *Polymer (Guildf)* 3269. <https://doi.org/10.1016/j.polymer.2011.05.029>
32. Chung CK, Lin YC, Huang GR (2005) Bulge formation and improvement of the polymer in CO<sub>2</sub> laser micromachining. *J Micromech Microeng* 15(10):1878–1884. <https://doi.org/10.1088/0960-1317/15/10/013>
33. Helmy MO, Fath El-Bab AM, El-Hofy H (2015) Elimination of clogging in PMMA microchannels using water assisted CO<sub>2</sub> laser micromachining. *Appl Mech Mater* 799–800:407–412. <https://doi.org/10.4028/www.scientific.net/amm.799-800.407>
34. Ravi-Kumar S, Lies B, Zhang X, Lyu H, Qin H (2019) Laser ablation of polymers: a review. *Polym Int* 68(8):1391–1401. <https://doi.org/10.1002/pi.5834>
35. Dowding C (2010) Laser ablation, in woodhead publishing series in welding and other joining technologies, J. Lawrence, J. Pou, D. K. Y. Low, and E. B. T.-A. in L. M. P. Toyserkani, Eds. Woodhead Publishing, p. 575–628. <https://doi.org/10.1533/9781845699819.7.575>
36. Shimamura A, Hotta Y, Hyuga H, Hotta M, Hirao K (2020) Improving the thermal conductivity of epoxy composites using a combustion-synthesized aggregated β-Si<sub>3</sub>N<sub>4</sub> filler with randomly oriented grains. *Sci Rep* 10(1):1–9. <https://doi.org/10.1038/s41598-020-71745-w>

## Authors and Affiliations

Heba Mansour<sup>1,2</sup>  · Emad A. Soliman<sup>2</sup> · Ahmed M. Fath El-Bab<sup>3</sup> · Ahmed L. Abdel-Mawgood<sup>1</sup>

Emad A. Soliman  
esoliman@srtacity.sci.eg

Ahmed M. Fath El-Bab  
ahmed.rashad@ejust.edu.eg

Ahmed L. Abdel-Mawgood  
ahmed.mawgood@ejust.edu.eg

<sup>2</sup> Department of Polymeric Materials, Advanced Technology and New Material Research Institute, City of Scientific Research and Technological Applications (SRTA-City), Alexandria 21934, Egypt

<sup>3</sup> Mechatronics and Robotics Department, School of Innovative Design Engineering, Egypt-Japan University of Science and Technology E-JUST, New Borg El-Arab City, Alexandria 21934, Egypt

<sup>1</sup> Biotechnology Department, Basic and Applied Sciences (BAS) Institute, Egypt-Japan University of Science and Technology (E-JUST), Alexandria 21934, Egypt